SECURITY INFORMATION

Copy 246

RM A51K14

[redacted]

NACA RM A51K14

[redacted]

TECH LIBRARY KAFB, NM

0142910

NACA

RESEARCH MEMORANDUM

EXPERIMENTAL INVESTIGATION OF THE EFFECT OF FOREBODY BLUNTNESS ON THE PRESSURE RECOVERY AND DRAG OF A TWIN-SCOOP INLET-BODY COMBINATION AT MACH NUMBERS OF 1.4 AND 1.7.

By John F. Stroud

Ames Aeronautical Laboratory
Moffett Field, Calif.

Unclassified

By Nasa Tech Pub Announcement #109

(AUTHORIZED TO CHANGE)

By 29 Nov 56

NK

GRADE OF

4 Apr. 61 CLASSIFIED DOCUMENT

DATE

This material contains information affecting

[redacted]

NATIONAL ADVISORY COMMITTEE FOR AERONAUTICS

WASHINGTON

February 14, 1952

319.98/13

[redacted]

TECH LIBRARY KAFB, NM
0142910

 [redacted]

NATIONAL ADVISORY COMMITTEE FOR AERONAUTICS

RESEARCH MEMORANDUM

EXPERIMENTAL INVESTIGATION OF THE EFFECT OF FOREBODY BLUNTNESS ON THE PRESSURE RECOVERY AND DRAG OF A TWIN-SCOOP INLET-BODY COMBINATION AT MACH NUMBERS OF 1.4 AND 1.7

By John F. Stroud

SUMMARY

The pressure recovery, mass flow, and drag of a twin-scoop inlet-body combination were measured at Mach numbers of 1.4 and 1.7 at zero angle of attack, and the results were presented in a preliminary data report. These data, in addition to some more recently obtained results of tests of the forebodies, are presented and analyzed in the present report. Tests were made of the inlet-body combination with an ogival forebody, with an ogival forebody having a small amount of bluntness near the tip, and with two forebodies of elliptic longitudinal section; the fineness ratios of the forebodies varied from 5 to 2.86. The results indicate that the effect on pressure recovery, mass-flow ratio, and drag of a small amount of bluntness of the ogival forebody was small. A very blunt forebody, however, combined with a relatively low fineness ratio, caused significant reductions in maximum pressure recovery and mass-flow ratio and a large increase in drag. At a Mach number of 1.7, the most blunt forebody when compared with the ogival forebody showed a loss in maximum pressure recovery of 0.06, a decrease in maximum mass-flow ratio of 0.06, and, for a mass-flow ratio of 0.90, an increase in drag of the inlet-body combination of about 135 percent. Similar results were obtained at a Mach number of 1.4. Tests of the various forebodies indicated that the variation of inlet location (forebody fineness ratio) with forebody bluntness affected the pressure recovery, mass-flow ratio, and scoop drag.

INTRODUCTION

A program to determine the practicability of twin-scoop inlets for the air-induction system of high-speed aircraft is in progress at the

[redacted]

Ames Aeronautical Laboratory. Information on the pressure recovery characteristics of this type of inlet mounted on a sharp-nosed forebody is presented in reference 1.

From aerodynamic considerations, a slender, nearly pointed forebody is desirable for the bodies of high-speed aircraft; however, the operation of radar equipment to be carried in the nose requires consideration of blunt bodies. Drag figures for bodies of revolution of four degrees of bluntness have been reported in reference 2, and some additional characteristics of the flow about blunt bodies at supersonic speeds have been presented in reference 3. An investigation of the effects of forebody bluntness on the pressure recovery, mass flow, and drag of a twin-scoop inlet-body combination has been made in order to assess the aerodynamic penalties involved in the use of a blunt forebody shape. The test results obtained for the inlet-body combinations were presented in reference 4. The data presented in reference 4 are analyzed and the results of subsequent tests in which the drag of the inlet-model forebodies and the total and static pressures ahead of the inlet station were measured are presented in this report.

NOTATION

A cross-sectional area, square feet

A_{ref} reference area (largest frontal area of model exposed to stream), square feet

a speed of sound, feet per second

C_{D_e} total external drag coefficient $\left\{ C_{D_e} = -\frac{F_G}{q_o A_{ref}} + \left[\frac{m(V_s - V_o) + (p_s - p_o)A_s}{q_o A_{ref}}\right] + \sum\left(P_{base}\frac{A_{base}}{A_{ref}}\right) - \sum\left(\Delta P_l \frac{\Delta A_{forebody}}{A_{ref}}\right)\right\}$

d duct station downstream of entrance, inches

F_G force measured by balance gage, pounds

H	total pressure $\left[p\left(1+\frac{\gamma-1}{2}M^2\right)^{\frac{\gamma}{\gamma-1}}\right]$, pounds per square foot absolute
M	Mach number $\left(\frac{V}{a}\right)$, dimensionless
m	mass-flow rate (ρVA), slugs per second
p	static pressure, pounds per square foot absolute
P	static-pressure coefficient $\left(\frac{p-p_o}{q_o}\right)$
q	dynamic pressure $\left(\frac{1}{2}\rho V^2\right)$, pounds per square foot
r	local forebody radius, inches
V	velocity, feet per second
X_n	distance forward of cylindrical section of forebody, inches
α	angle of attack, degrees
γ	ratio of specific heats, dimensionless
ρ	mass density, slugs per cubic foot

Subscripts

av	average
A,C,D	forebodies A, C, and D
o	free stream
o'	station on forebody without inlets corresponding to station 0.150 inch ahead of inlets
o''	station on body where static pressure corresponds to that recovered on forebody A at station o'
max	maximum

1 inlet station

3 settling chamber

4 exit throat

l station on forebody

MODELS

The scoop inlets were tested in combination with four forebody shapes, each having a different fineness ratio. The forebody of the basic model (forebody A, fig. 1) consisted of a 10-caliber ogival nose of circular cross section followed by a cylindrical section to the inlet ramp. Nose B was parabolic in longitudinal section and became tangent to the basic ogive 0.50 inch from the basic forebody tip. Forebodies C and D were elliptic in shape with the points of tangency to the basic body occurring at the beginning of the cylindrical section. On the basic model (forebody A) the twin-scoop inlets were located five body diameters behind the apex of the ogive and enclosed approximately 19 percent of the maximum circumference of the forebody. The inlet area, including both scoops, was 18.2 percent of the total frontal area immediately aft of the inlet station. The maximum frontal area of the inlet-body combination, on which all drag coefficients are based, was 0.638 square inch. As shown in figure 1, each scoop was preceded by a 4° ramp. A sharp edge was used on the duct lips with the external surface inclined 5° to the duct plane of symmetry at the side walls and 3° at the outer surfaces. The duct passage consisted of a constant area section for a length of two inlet heights aft of the entrance, followed by a diverging diffuser. The internal cross-sectional-area variation with distance from the duct entrance is presented in figure 2.

Separate models of forebodies C and D, shown in figure 3, were provided for pressure surveys just ahead of the inlet station. These models, with the pressure rake removed, were also used to measure the drag of the portions of the bodies ahead of the inlets. The lengths of the models were equal to the distances from the apexes to the inlet station on the corresponding inlet-body combinations.

TESTS AND PROCEDURE

The tests were conducted in the Ames 8- by 8-inch supersonic wind tunnel. A detailed description of the tunnel and its auxiliary equipment is presented in reference 5. Pressure recovery, mass flow, and drag of

twin-scoop inlet-body combinations were measured at Mach numbers of 1.4 and 1.7 at zero angle of attack. Total and static pressure surveys were made just ahead of the inlet station at distances of 0.050, 0.100, 0.150, and 0.200 inch from the surfaces of forebodies C and D. The measurements were made ahead of both inlets for each tube, at the distances mentioned, by rotating the forebody models (fig. 3). In addition, the drag of the bodies ahead of the inlets was measured. All measurements were made at Reynolds numbers per foot of length of approximately 8 and 9 million at Mach numbers of 1.4 and 1.7, respectively.

The support system and instrumentation used to obtain simultaneous measurements of pressure recovery, mass flow, and drag force are shown in figure 4 and are described in reference 6. The internal survey rake, which could be rotated, consisted of four total-pressure tubes and three static-pressure tubes. The same drag balance was used to measure forebody drag that was used to measure the drag of the inlet-body combination. However, the shroud shown in figure 3 was used to fair the bases of the bodies without inlets into the stationary outer shell. Drag forces acting on the strain-gage balance were obtained from deflections of a dynamically balanced galvanometer.

All pressures measured in this investigation were photographically recorded from a multiple-tube mercury manometer. Readings of the internal pressure-survey rake were recorded at 10 angular positions of the rake for each mass-flow ratio. Flow about the models was observed and photographed through a schlieren apparatus having a knife edge parallel to the free stream.

REDUCTION OF DATA

The total-pressure ratio H_3/H_0 that is used in the data presentation is an average weighted on the basis of annular areas of approximately equal width assigned to each survey tube of the rake in the model settling chamber. The total-pressure ratio H_0'/H_0 was obtained from pressure readings which were corrected for normal shock losses.

The mass-flow ratio, defined as the ratio of mass flowing through the diffuser to that flowing in the free stream through an area equal to that of the entrance, was calculated by the following relation:

$$\frac{m_1}{m_0} = \left(\frac{H_3}{H_0}\right)_{av} \times \frac{A_4}{A_1} \times \frac{1}{M_0} \left(\frac{2}{\gamma+1} + \frac{\gamma-1}{\gamma+1} M_0^2\right)^{\frac{\gamma+1}{2(\gamma-1)}} \times K$$

The correction factor K, which was a function of outlet plug position, was determined by calibration.

The total external drag force of the inlet-body combination is defined as the algebraic sum of the change in total momentum between the free stream and the inlet station of the mass of air that flowed through the inlet and the external pressure and friction forces acting on the model in the axial direction. Corrections were applied to the drag data to account for all buoyancy forces on the model and balance.

A detailed discussion of accuracy of the test apparatus is contained in reference 6. The drag coefficients have been estimated to be accurate within ±0.008; however, the scatter of the data for the inlet-body combination with forebody D at Mach number 1.7 is in excess of this value. The exact cause of excessive experimental scatter in these particular data is unknown; however, it was believed to be due to an increase in balance friction which developed during this final run. Repeating this run was impractical because of damage sustained by the model at the conclusion of the test. The estimated accuracy of the drag data includes the possible error due to different skin-friction conditions on the various models. Estimates of the accuracy of the remaining parameters are tabulated below:

Parameter	Estimated accuracy
Pressure recovery H_3/H_o	±0.005
Mass-flow ratio m_1/m_o	±.015
Mass-velocity ratio $\frac{\rho_o' V_o'}{\rho_o V_o}$	±.005

RESULTS AND DISCUSSION

Effect of Forebody Bluntness on Pressure Recovery

The variations of total pressure recovery with mass-flow ratio for the scoop inlets preceded by forebodies of various degrees of bluntness are presented in figure 5. The losses in total pressure recovery increased with increasing forebody bluntness and Mach number. The inlet-body combination with the largest degree of forebody bluntness and the smallest fineness ratio sustained losses in maximum total pressure recovery of about 0.03 and 0.06 above those of the combination with the ogival forebody, at Mach numbers of 1.4 and 1.7, respectively. The flow fields around the blunt body (forebody D) for these conditions are illustrated

by schlieren photographs (fig. 6) for comparison with those of the sharp-nosed forebody.

The variations of the total-pressure ratio $\frac{H_o'}{H_o}$ with radial distance from the bodies are shown in figure 7 for forebodies C and D. The integrated total-pressure losses measured over the inlet height at station o' increase with increasing forebody bluntness because an increasing mass of air is affected by the strong parts of the bow shock wave. This effect can be seen by comparison between forebodies C and D of the total-pressure losses and vertical total-pressure gradients at station o' (fig. 7).

In order to present the total-pressure decrements due to forebody bluntness, the data of figure 7 were numerically averaged from the data points shown to represent the percentage of free-stream total pressure available to the inlets. The decrements in total pressure due to forebody bluntness $\frac{H_o-H_o'}{H_o}$ (measured ahead of inlets) and the decrements in total pressure between stations o' and 3 for constant values of mass-flow ratio are tabulated below:

Free-stream Mach number	Forebody	$\frac{H_o-H_o'}{H_o}$	m_1/m_o	$\frac{H_o'-H_3}{H_o'}$
1.4	A	0	0.6	0.135
↓	C	.019	↓	.142
	D	.026		.146
1.7	A	0	.8	.232
↓	C	.035	↓	.234
	D	.090		.209

In this tabulation, the assumption was made that H_o' for forebody A was equal to H_o. The error in $\frac{H_o'-H_3}{H_o'}$ introduced by this assumption, according to shock-wave theory, is approximately 0.002. The decrements in total pressure due to forebody bluntness $\frac{H_o-H_o'}{H_o}$ do not include losses in the boundary layer. Calculations of the laminar boundary-layer growth on cones having the same fineness ratios as the various forebodies indicate that at station o' the variations in thickness with forebody length produce differences in the boundary layer which would result in a change of less than 0.005 in $\frac{H_o-H_o'}{H_o}$.

The tabulated decrements in total pressure between stations o' and 3 include an error resulting from the fact that H_o' does not include boundary layer losses. Estimates indicate that this error in $\frac{H_o'-H_3}{H_o'}$ is probably less than 0.01. The preceding table shows that the losses in total pressure ahead of the inlet $\frac{H_o-H_o'}{H_o}$ increase much faster with increasing forebody bluntness at Mach number 1.7 than at Mach number 1.4. The tabulation of losses in total pressure within the inlet $\frac{H_o'-H_3}{H_o'}$, however, indicates a decrease in diffuser losses, at Mach number 1.7, between the combination with the sharp-nosed forebody (A) and the combination with the most blunt forebody (D) of reduced fineness ratio. The diffuser total-pressure loss $\frac{H_o'-H_3}{H_o'}$ remained practically constant between forebodies A and C (at $M_o = 1.7$) for a reduction in local Mach number of about 1-1/2 percent, while a decrease in the diffuser total-pressure loss (increase in pressure recovery) of 0.023 is indicated between forebodies A and D for a reduction in local Mach number of about 3 percent. The trend of these data for Mach number 1.7 indicates that factors in addition to local Mach number ahead of the inlet were responsible for the variation in diffuser pressure recovery noted. It is believed that the principal additional factors involved were related to shock-wave boundary-layer interaction since the different pressure distributions and lengths of the forebodies probably caused variations in the profile of the boundary layer and hence influenced the tendency of the flow to separate in the diffuser compression system.

Effect of Forebody Bluntness on Mass-Flow Ratio

The losses in maximum mass-flow ratio for the inlets with forebodies of various degrees of bluntness are indicated in figure 5. In order to illustrate the effect of forebody bluntness on mass-flow ratio, the concept of mass velocity, ρV, is introduced. The mass velocity just ahead of the inlets, $\rho_o'V_o'$, is a measure of the mass flow per unit area available to the inlets. This mass velocity was calculated for forebodies C and D from total and static pressure measurements obtained 0.150 inch ahead of the inlets. The decrements in maximum mass-flow ratios $\frac{\rho_1 V_1 A_1}{\rho_o V_o A_1}$ and in mass-velocity ratios $\frac{\rho_o' V_o'}{\rho_o V_o}$ are tabulated below for comparison:

[redacted]

Mach number M_o	$\dfrac{\left(\frac{m_1}{m_o}\right)_{max_A} - \left(\frac{m_1}{m_o}\right)_{max_C}}{\left(\frac{m_1}{m_o}\right)_{max_A}}$	$\dfrac{\left(\frac{m_1}{m_o}\right)_{max_A} - \left(\frac{m_1}{m_o}\right)_{max_D}}{\left(\frac{m_1}{m_o}\right)_{max_A}}$
1.4	0.036	0.045
1.7	.038	.065

Mach number M_o	$\dfrac{(\rho_o'V_o')_A-(\rho_o'V_o')_C}{\rho_oV_o}$	$\dfrac{(\rho_o'V_o')_A-(\rho_o'V_o')_D}{\rho_oV_o}$
1.4	0.027	0.043
1.7	.017	.050

(As noted previously, the estimated accuracies of the mass-flow ratio and the mass-velocity ratio are ±0.015 and ±0.005, respectively.) The values in the preceding table indicate that the losses in maximum mass flow are primarily due to the losses in mass velocity (reduction in available mass flow per unit area) rather than to the spillage associated with a detached shock wave at the inlet lip. The reductions in mass velocity arising from forebody bluntness are due to the entropy rise across the strong detached bow waves. After the flow has progressed far enough along the body to recover free-stream static pressure, the increase in entropy is manifest as a loss in velocity and a decrease in density caused by the rise in static temperature.

Part of the losses in mass velocity, and thus mass flow, at Mach number 1.4 were a result of the fact that the static pressures measured ahead of the inlets were lower than those on forebody A. (Static pressure measurements made on forebody A at station o' indicated losses of 1.5 and 2.6 percent, at free-stream Mach numbers of 1.4 and 1.7, respectively, of free-stream mass velocity as a result of locating the inlets in a region of static pressure lower than the free-stream value.) The remainder of the losses were due to the total-pressure losses associated with the entropy rise across the detached bow waves. In order to separate the losses into the two components, the total pressures measured ahead of the inlets with the blunt forebodies were used with the static pressure measured ahead of the inlets on forebody A to calculate the losses in mass velocity due to forebody bluntness. The results of this calculation are presented below:

Free-stream Mach number M_o	$\frac{(\rho_o'V_o')_A-(\rho_o''V_o'')_C}{\rho_oV_o}$	$\frac{(\rho_o'V_o')_A-(\rho_o''V_o'')_D}{\rho_oV_o}$
1.4	0.013	0.021
1.7	.023	.042

Comparison of the values of this table with those of the previous table indicates that at a Mach number of 1.4 about half the loss in mass velocity was due to the fact that the inlets were located in a region of low static pressure. However, at a Mach number of 1.7 this effect is practically negligible, relative to forebody A, and the loss in mass velocity is due to the loss in total pressure through the strong bow shock wave. Losses in mass velocity, and thus mass flow, whether due to forebody bluntness or fineness ratio (inlet location), must be considered in matching an inlet and an engine whose air requirements are based on free-stream conditions.

In general, in order to obtain the maximum available mass-flow ratio and pressure recovery for any scoop inlet (preceded by a forebody of the compression-expansion-compression type employed in the present investigation) in an inviscid fluid, the inlet must be preceded by a forebody of sufficient fineness ratio to permit recovery of free-stream static pressure.

Effects of Forebody Bluntness on Drag

Drag curves for the inlet-body combinations and for the bodies without inlets are presented in figure 5 for Mach numbers of 1.4 and 1.7. All the drag coefficients are based on the maximum frontal area of the inlet-body combination.

The smallest degree of forebody bluntness (forebody B) produced a very slight increase in drag of the inlet-body combination at Mach numbers of 1.4 and 1.7. The fact that this drag rise was so small can probably be attributed to an overexpansion of the flow following the sonic point on the rounded nose, thus permitting the effect of the positive pressures on the rounded nose to be approximately counterbalanced by the negative pressures acting farther downstream on the forebody. Large rises in drag occurred between forebodies A and C and forebodies A and D, as shown in figure 5. These large drag increases are probably attributable to the fact that for these very blunt bodies the sonic point was so far removed from the body axis (reference 3) that the forces on the extensive region of the frontal area exposed to high positive pressures in a subsonic flow field were not counterbalanced by the forces in the region of expansion downstream of the sonic point.

The total and static pressure surveys ahead of the inlet station showed that at Mach number 1.4 the effect of forebody bluntness, combined with the reduced fineness ratio, was to decrease both pressures. The local Mach number was almost unaffected since both pressures decreased nearly proportionately. The scoop drag (defined as the difference between the total external drag of the inlet-body combination and the drag of the forebody ahead of the inlets) reduction with increasing forebody bluntness at Mach number 1.4 (fig. 5(a)) is probably due to the local decrease in static pressure on the external scoop surfaces. The scoop drag remained essentially constant with forebody bluntness at Mach number 1.7 (fig. 5(b)) because the measured static pressure and Mach number just ahead of the inlets changed only slightly.

CONCLUDING REMARKS

Wind-tunnel tests were performed at Mach numbers of 1.4 and 1.7 at zero angle of attack on a twin-scoop inlet-body combination with forebodies of various degrees of bluntness. The losses in pressure recovery increased with increasing forebody bluntness and Mach number. The largest degree of forebody bluntness, as compared to the ogival forebody, caused losses in maximum pressure recovery of about 0.03 and 0.06 for the inlet-body combination at Mach numbers of 1.4 and 1.7, respectively. The corresponding losses in maximum mass-flow ratios were about 0.04 and 0.06. The losses in maximum mass-flow ratio at Mach number 1.7 were primarily due to the losses in total pressure through the bow wave, while those at Mach number 1.4 were due approximately one-half to total pressure loss and one-half to the fact that the inlets were located in a region of low static pressure.

The drag of the inlet-body combination increased markedly with increasing forebody bluntness, but only slightly with increasing Mach number. At a Mach number of 1.7 and a mass-flow ratio of 0.90, the largest degree of forebody bluntness tested caused an increase in drag of the inlet-body combination of about 135 percent. A reduction in scoop drag with increasing forebody bluntness was observed at Mach number 1.4; this was believed to be a result of lowered static pressure just ahead of the inlets.

Ames Aeronautical Laboratory,
National Advisory Committee for Aeronautics,
Moffett Field, Calif.

REFERENCES

1. Davis, Wallace F., Edwards, Sherman S., and Brajnikoff, George B.: Experimental Investigation at Supersonic Speeds of Twin-Scoop Duct Inlets of Equal Area. IV - Some Effects of Internal Duct Shape Upon an Inlet Enclosing 37.2 Percent of the Forebody Circumference. NACA RM A9A31, 1949.

2. Hart, Roger G.: Flight Investigation of the Drag of Round Nosed Bodies of Revolution at Mach Numbers from 0.6 to 1.5 Using Rocket-Propelled Test Vehicles. NACA RM L51E25, 1951.

3. Moeckel, W. E.: Experimental Investigation of Supersonic Flow with Detached Shock Waves for Mach Numbers Between 1.8 and 2.9. NACA RM E50D05, 1950.

4. Stroud, John F., and Anderson, Warren E.: Preliminary Data on the Effect of Body-Nose Bluntness on the Drag and Pressure Recovery of a Side-Inlet-Body Combination at Mach Numbers of 1.4 and 1.7. NACA RM A51A09, 1951.

5. Davis, Wallace F., Brajnikoff, George B., Goldstein, David L., and Spiegel, Joseph M.: An Experimental Investigation at Supersonic Speeds of Annular Duct Inlets Situated in a Region of Appreciable Boundary Layer. NACA RM A7G15, 1947.

6. Brajnikoff, George B., and Rogers, Arthur W.: Characteristics of Four Nose Inlets as Measured at Mach Numbers Between 1.4 and 2.0. NACA RM A51C12, 1951.

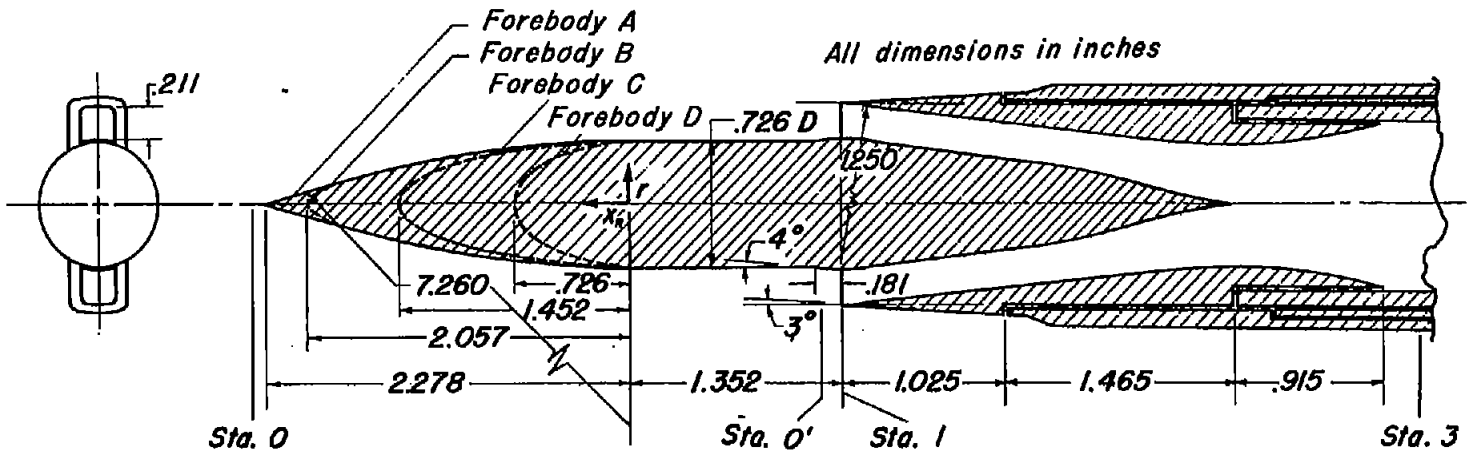

Forebody B	
x_n	r
1.778	0.141
1.817	0.131
1.857	0.119
1.882	0.112
1.907	0.103
1.932	0.094
1.957	0.084
1.987	0.071
2.002	0.063
2.017	0.053
2.032	0.042
2.042	0.033
2.057	0

Forebody C	
x_n	r
0	0.363
0.250	0.358
0.500	0.341
0.750	0.311
1.000	0.263
1.100	0.237
1.200	0.204
1.300	0.162
1.350	0.134
1.375	0.117
1.400	0.096
1.415	0.081
1.425	0.070
1.435	0.055
1.452	0

Forebody D	
x_n	r
0	0.363
0.100	0.360
0.200	0.349
0.300	0.330
0.400	0.303
0.450	0.285
0.500	0.263
0.550	0.237
0.600	0.204
0.650	0.162
0.675	0.134
0.685	0.120
0.700	0.096
0.710	0.076
0.726	0

NACA

Figure 1. – Model dimensions.

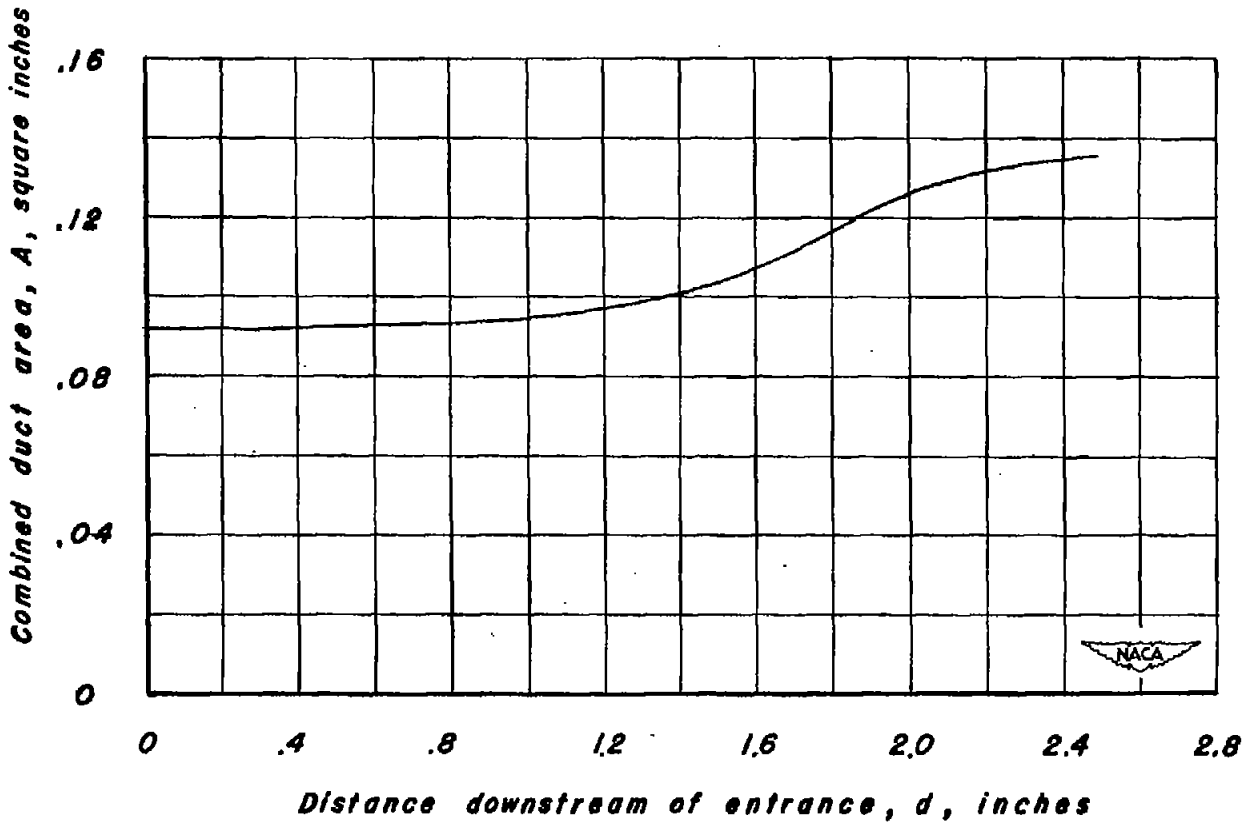

Figure 2.- Internal duct area variation.

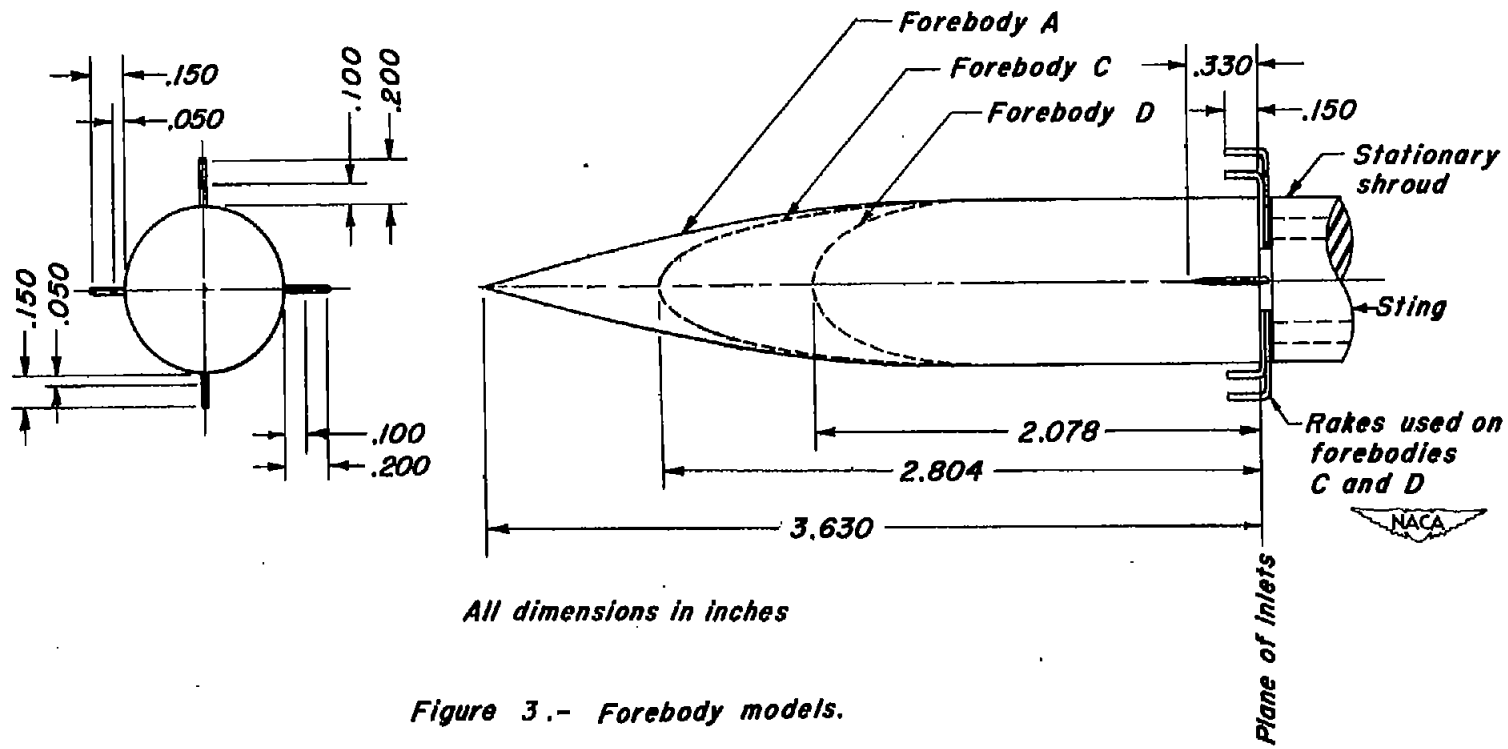

Figure 3.- Forebody models.

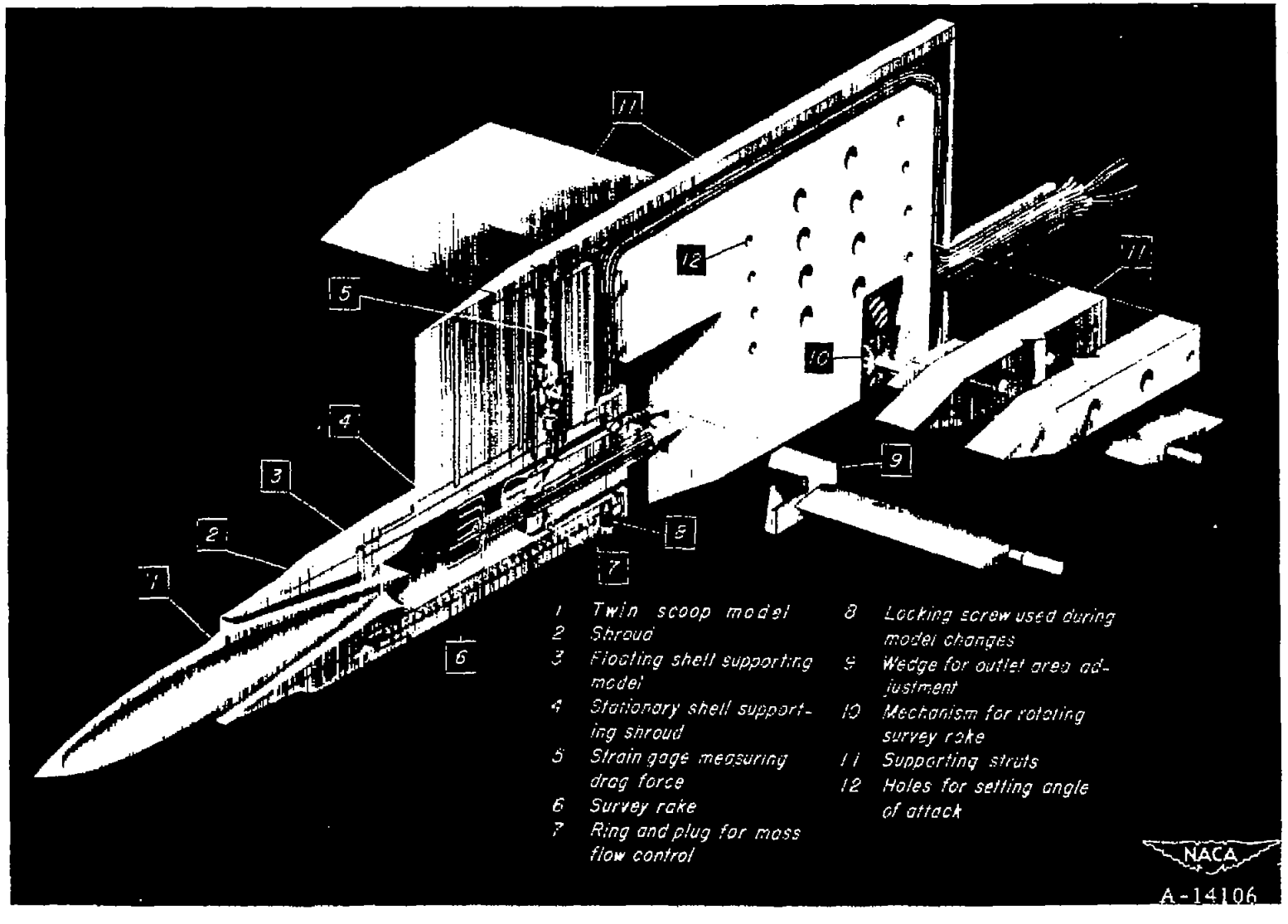

Figure 4.– Apparatus for measuring the performance of supersonic duct inlets.

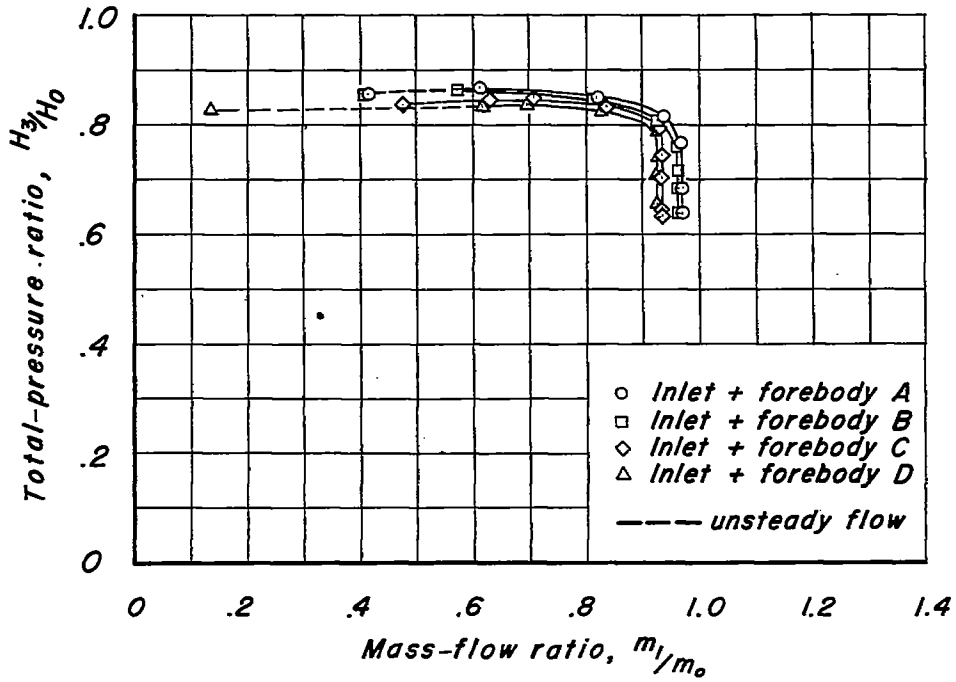

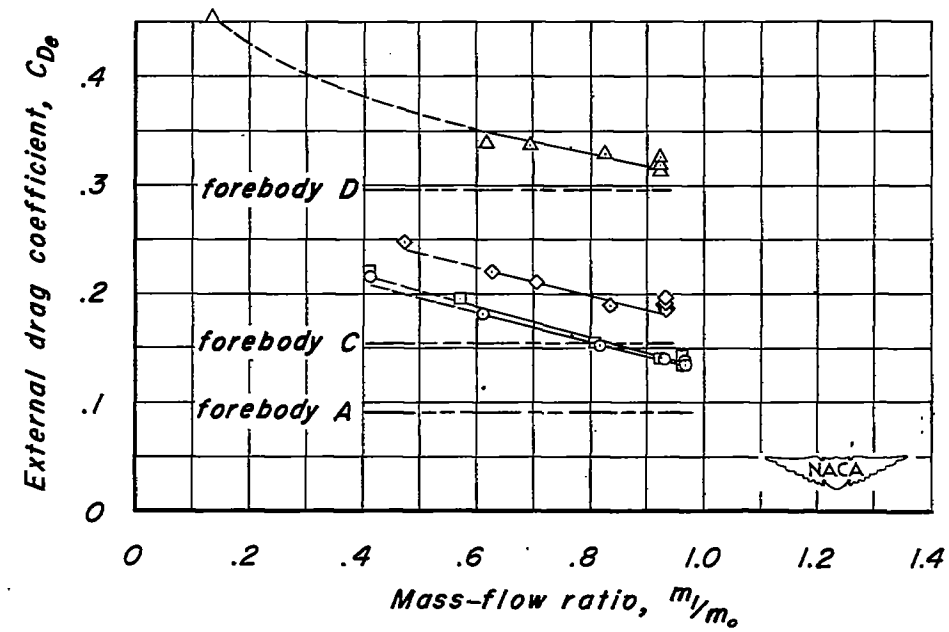

(a) $M_0 = 1.4$, $\alpha = 0°$

Figure 5.- Variation of total-pressure recovery and external drag coefficient with mass-flow ratio for four forebody configurations.

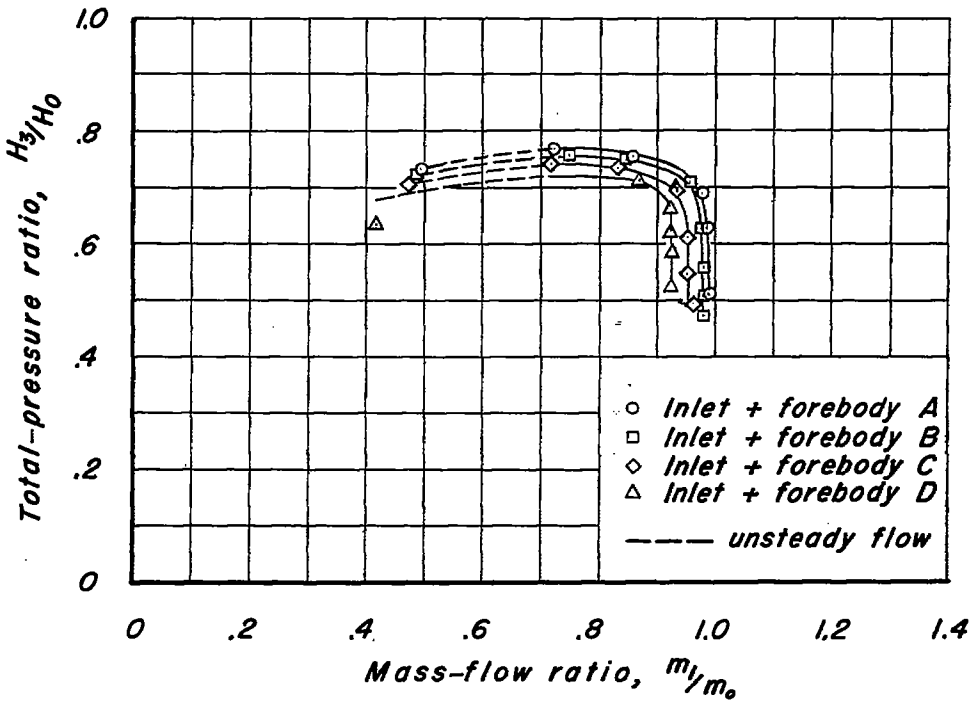

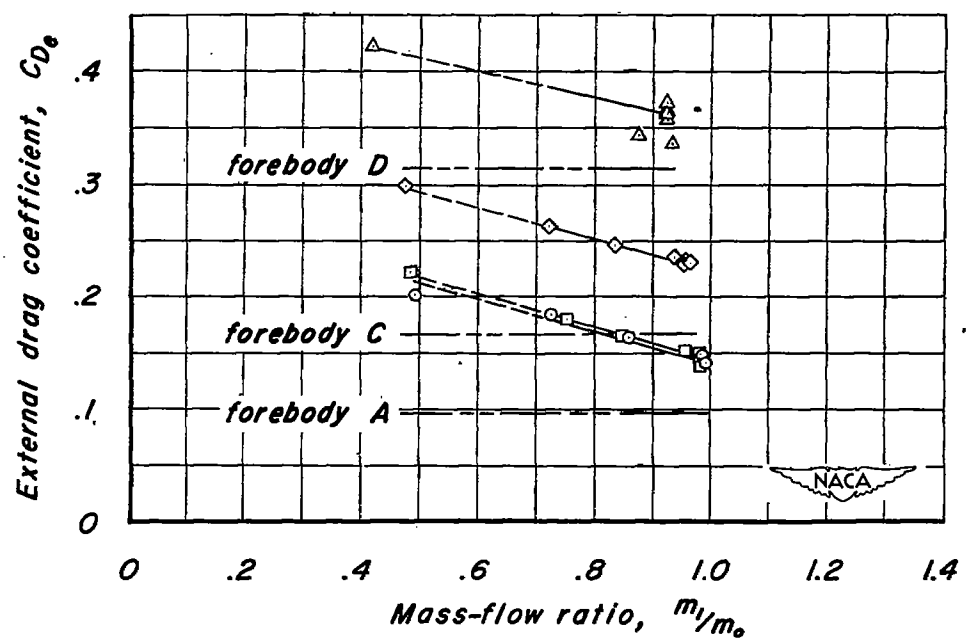

(b) $M_0 = 1.7$, $\alpha = 0°$

Figure 5.- Concluded.

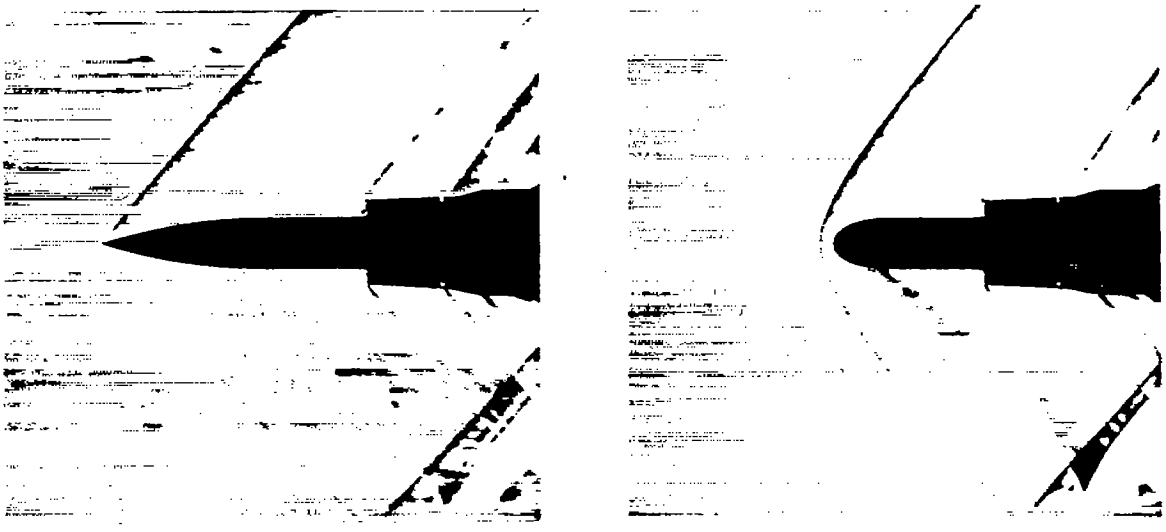

Forebody A
$(m_1/m_o)_{max}$=0.970

Forebody D
$(m_1/m_o)_{max}$=0.925

(a) M_o=1.4

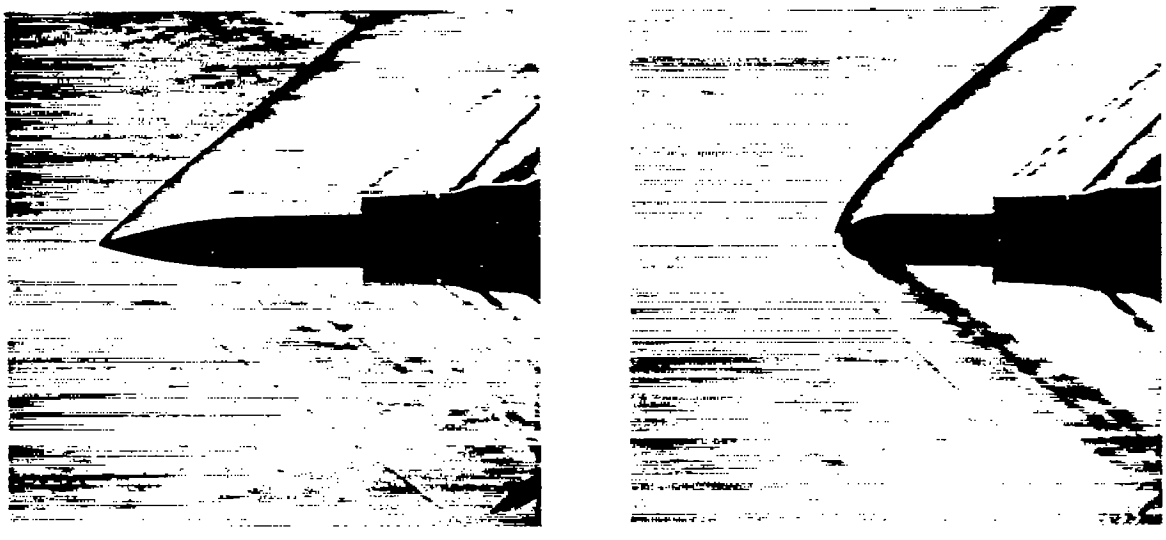

Forebody A
$(m_1/m_o)_{max}$=0.990

Forebody D
$(m_1/m_o)_{max}$=0.925

(b) M_o=1.7

Figure 6.– Schlieren photographs of model with forebodies A and D.

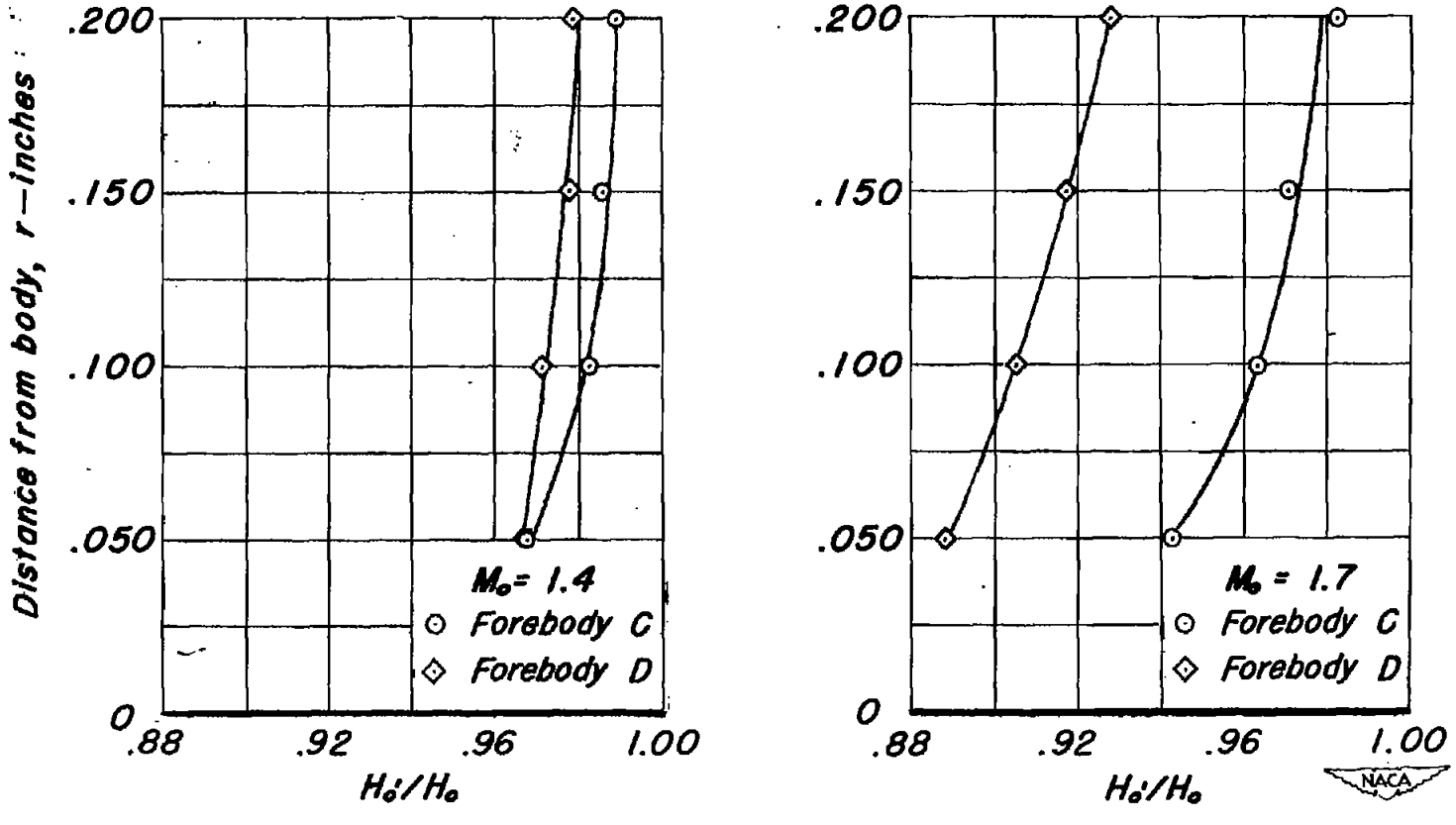

Figure 7. – Variation of total-pressure ratio with distance from body 0.150 inch ahead of inlet.